Full Paper Wiley Online Library ELECTROANALYSIS

DOI: 10.1002/elan.202060163

Cyclic Voltammetric Study of 2-Hydroxybenzophenone (HBP) Derivatives and the Correspondent Change in the Orbital Energy Levels in Different Solvents

Adebayo A. Adeniyi,*[a, b] Tankiso L. Ngake,[a] and Jeanet Conradie*[a, c]

Abstract: The experimental UV and CV of five substituted 2-hydroxybenzophenones in solvents acetonitrile, n-dimethylformamide and dimethylsulfoxide are presented. Results obtained were used to determine their experimental highest occupied molecular orbital (HOMO) and lowest unoccupied molecular orbital (LUMO) and the results were compared to their theoretical model. The derivatives with an electron withdrawing group (EWG) have more favourable reduction potential, electron affinity, lower dipole moment, lower LUMO and HOMO energy levels and longer absorption λ_{max} compared to those containing an electron donating group. Acetonitrile enhances the reduction potential especially for those of derivatives with EWG, leading to higher reduction potential compared to solvents DMF and DMSO.

Keywords: 2-Hydroxybenzophenone · reduction · DFT · UV/vis · HOMO/LUMO

1 Introduction

2-Hydroxybenzophenone (HBP) molecules have been considered in many studies due to their application as a UV chromophore in many commercial sunscreens [1–4]. HBP derivatives are believed to be photostable and lack reactivity even after several hours of irradiation [1,5]. The photostability is due to their major energy-wasting deactivation process through excited-state intramolecular proton transfer from the chelated enol to the chelated keto form [6]. The enol form has been identified to be the only one minimum in the ground state while the chelated keto form identified to be the minimum in the excited state [6,7]. Available solid state crystal structures of HBP and related ligands are all of the chelated enol form [8–13].

The optical bandgap of molecules is very important for their photoexcitation properties and it can be determined using experimental UV-Vis spectroscopy. The values of the optical bandgap are known to be close to the electronic gap (electrochemical HOMO-LUMO gap) [14,15]. It has been established for many organic semiconductor molecules that the electronic bandgap calculated with DFT is very close in value to the optical bandgap [16]. The experimental highest occupied molecular orbital (HOMO) and lowest unoccupied molecular orbital (LUMO) can be estimated from the plot of the first oxidation and first reduction potential obtained by cyclic voltammetry (CV) respectively. It is also experimentally possible to determine the HOMO-LUMO gap energies from absorption and reflectance spectra obtained through electrical conductivity measurements and photoconductivity techniques [17–19]. The control of HOMO-LUMO energy gap of π-conjugated systems is known to be critical task for the semiconductor and nanomaterial industries [16,20,21]. Knowledge of the UV-Vis HOMO-LUMO gap is important to determine the effectiveness of HBP to absorb in the UV-Vis region to act as sunscreen.

2-Hydroxybenzophenone is a suitable recyclable, inexpensive, and readily removable chemical auxiliary in the organocatalytic activation of ketiminoesters for highly enantioselective addition to nitroalkenes under bifunctional catalysis [22]. Knowledge of the redox properties of a molecules is important for its use in catalytic processes.

In this research the experimental reduction potential (using cyclic voltammetry (CV)) and UV/vis spectra, of the five HBP molecules shown in Figure 1, 5-bromo-2-hydroxybenzophenone (1), 5-chloro-2-hydroxybenzo-

[a] A. A. Adeniyi, T. L. Ngake, J. Conradie
Department of Chemistry, University of the Free State, PO Box 339, Bloemfontein, 9300, South Africa
Tel.: +27 717873258
E-mail: AdeniyiAA@ufs.ac.za
conradj@ufs.ac.za
[b] A. A. Adeniyi
Department of Industrial Chemistry, Federal University of Oye-Ekiti, Nigeria
[c] J. Conradie
Department of Chemistry, UiT – The Arctic University of Norway, Tromsø N-9037, Norway.

Supporting information for this article is available on the WWW under https://doi.org/10.1002/elan.202060163

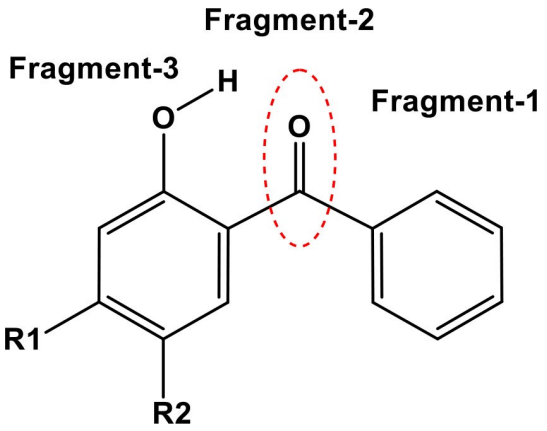

Fig. 1. Structure of the 2-hydroxybenzophenone derivatives 1 (5-Br, R1 = H, R2 = Br), 2 (5-Cl, R1 = H, R2 = Cl), 3 (R1 = H, R2 = H), 4 (4-OMe, R1 = OCH_3, R2 = H), 5 (4-Oct, R1 = $OC_{10}H_{21}$, R2 = H). The dotted oval indicates the plane of fragmentation into three fragments, Fragment-1, Fragment-2 and Fragment-3.

phenone (2), 2-hydroxybenzophenone (3), 2-hydroxy-4-methoxybenzophenone (4) and 2-hydroxy-4-(octyloxy) benzophenone (5), are presented in three different solvents, namely acetonitrile (ACN), n-dimethylformamide (DMF) and dimethylsulfoxide (DMSO). The experimental HOMO-LUMO gaps are determined from the CV and UV/vis data and compared to density functional theory (DFT) calculated HOMO and LUMO energies. The DFT calculated frontier orbitals showed the character of the reduction centre (LUMO) and provide the energy of the lowest UV/vis excitation of the molecules.

2 Methodology

2.1 Experimental Cyclic Voltammetry

A concentration of 0.002 mol dm^{-3} (or saturated) solutions of each HBP derivatives was used for the cyclic voltammetry measurement in dry ACN, DMF and DMSO solvents. The supporting electrolyte used is 0.1 mol dm^{-3} tetra-n-butylammoniumhexafluorophosphate (nBu_4N)(PF_6) and the experiment were carried out under a blanket of purified argon gas at 25 °C. A glassy carbon (surface area 7.07×10^{-6} m^2) was used as a working electrode; Pt as auxiliary electrode while the reference electrode is Ag/Ag^+ (0.010 mol dm^{-3} $AgNO_3$) mounted on a Luggin capillary. All CVs were measured with and without Fc as internal standard. All the CV potentials are referenced against the ferrocene/ferrocenium couple Fc/Fc^+, as suggested by IUPAC [23]. The reduction potential values $E^{0'}$ were determined as $E^{0'} = (E_{pa} + E_{pc})/2$ and the peak separation $\Delta E_p = (E_{pa} - E_{pc})$ with E_{pa}/E_{pc} = peak anodic/cathodic potential of the reduction wave. Successive experiments under the same experimental conditions showed that all peak reduction potentials were reproducible within 0.005 V. Scan rates were 0.05–5.00 Vs^{-1}.

2.2 Experimental E_{gap}, HOMO and LUMO

Depending on the type of the molecules, the HOMO can be derived from the onset potential of the first oxidation peak while the LUMO can be derived from the onset potential of the first reduction peak [15,24]. The onset value of the first reduction peak, obtained from the CV plot is shown in Figure 2 for molecule 1 in solvent ACN medium. The molecules considered in this study are characterised with reduction potential peaks according to the CV analysis, therefore the LUMO were first calculated using the expression [18]:

$$\begin{aligned} E_{LUMO} &= -IP\ V = \{-E'_{red/onset} - IP(reference)\}\ eV \\ &= \{-E'_{red/onset} - E_{1/2}(Fc/Fc^+) - (IP(Fc))\} eV \\ &= \{-E'_{red/onset} - IP(Fc) eV \end{aligned} \quad (1)$$

since values in this study were reported *vs* Fc/Fc^+ as reference, thus $E_{1/2}(Fc/Fc^+)$ is already added in shifting the CV plot with respect to Fc/Fc^+. The internal standard redox of the system is represented as IP(Fc) and is taking to be 4.80 [24,25].

An electronic band gap ($E_{gap,\ electronic}$) is the difference in energy between the highest occupied electron state and the lowest unoccupied electron state at zero

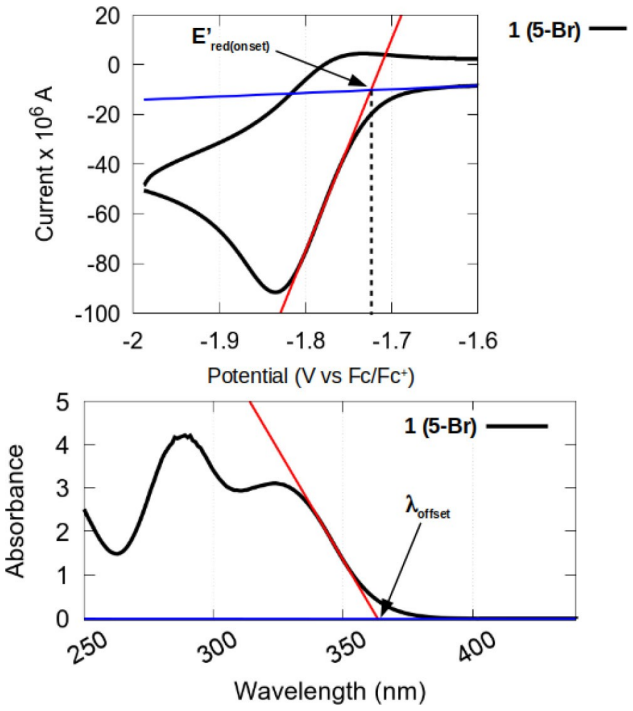

Fig. 2. The experimental (a) CV and (b) UV of 1 (5-Br) in ACN solvent showing the determination of the onset and offset positions that were used to calculate the experimental HOMO and LUMO energy levels

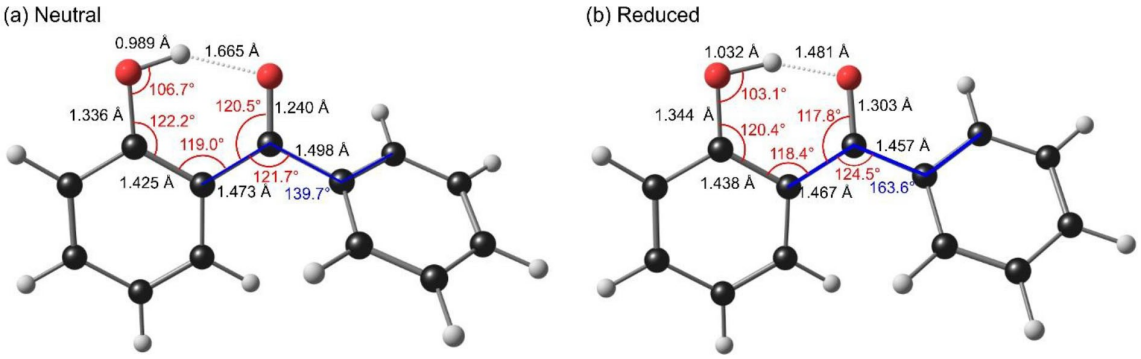

Fig. 3. B3LYP/6-31+G(2df,2p) gas phase optimized neutral and reduced geometry of 3. Selected bond lengths (Å, black), angles (°, red) and dihedral angle (°, blue) are indicated. Colour code (online version): C (black), O (red), H (white).

temperature. The experimental HOMO of each molecule was computed from their experimental electronic band gap ($E_{gap,\ electronic}$) and the LUMO (obtained from equation 1) as

$$E_{HOMO} = E_{LUMO} + E_{gap,\ electronic} \quad (2)$$

The optical band gap $E_{gap,\ optical}$ is the lowest energy for which a photon can be absorbed or emitted by a single photon process which conserves. The values of $E_{gap,\ optical}$ were obtained from the onset wavelength of the UV-Vis spectra using the expression:

$$E_{gap,\ optical} = h \times f = h \times c/\lambda_{offset} = 1240/\lambda_{offset} \quad (3)$$

The $E_{gap,optical}$ represents the optical band gap in eV and λ_{offset} in nm represent the absorption edge wavelength obtained from the offset wavelength of the low energy absorption band [16] as shown below (Figure 2b) for molecule 1 in ACN. Since for many organic semiconductor molecules the electronic bandgap calculated with DFT is very close in value to the optical bandgap [16], we used $E_{gap,\ electronic} = E_{gap,\ optical} = E_{gap}$.

2.3 Computational Calculations

The geometries of the neutral and reduced molecules were optimized in the gas phase, using density functional theory (DFT) with the B3LYP functional and all electron basis set 6-31+G(2df,2p) using Gaussian 16 [26]. Single point/6-31+G(2df,2p) calculations in the solvents ACN, DMF and DMSO, using the Solvation Model based on Density (SMD) with default parameters, provided electronic energies and dipole moment. The electron affinity EA was determined from the difference between the electronic energies of the neutral and reduced optimized molecules. The SMD solvation model is based on density (SMD) [27], as the polarizable continuum model (PCM) which applies the integral equation formalism variant (IEF-PCM), to solve the non-homogeneous Poisson equation with optimized atomic coulomb radii and non-electrostatic terms, from parameters that include the solvent accessible surface area, as well as atomic and molecular surface tensions [28]. The UV was computed using time dependent density functional method TD-B3LYP and the basis set 6-31+G(2df,2p) in the specified solvent.

3 Results and Discussion

3.1 DFT Calculated Geometry and Properties of Molecules

The geometry of the neutral and reduced HBP molecules, 1–5 (Figure 1) were optimized at the B3LYP/6-31+G(2df,2p) level of theory in the gas phase, the optimized coordinates are added in the supplementary information. Figure 3 show selected geometrical parameters of the optimized neutral and reduced molecule 3. Both the neutral and reduced molecule are flat with only the phenyl ring twisted out of the flat plane (139.7° and 163.6° respectivily), similar as was found for the neutral molecule in the solid state [9]. Upon reduction enol H gets nearer to the keto O and the dihedral involving the phenyl ring rotation increases with ca 20°, nearing the flat plane (dihedral 180°).

The values of the calculated electron affinity of 1–5 in the three solvents, as well as their dipole moments are given in Table 1. The electron withdrawing substituent group increase the electron affinities of the derivatives, leading to the order of molecule 2 (largest value) $\approx 1 > 3 > 4 > 5$ regardless of the solvent. Thus

Table 1. The electronic affinity (eV) and free energy of dipole moment (debye) of 1–5 in solvent ACN, DMF and DMSO.

	Electronic affinity (eV)			Dipole moment (debye)		
	ACN	DMF	DMSO	ACN	DMF	DMSO
1 (5-Br)	2.70	2.68	2.69	7.367	7.298	7.315
2 (5-Cl)	2.71	2.69	2.70	6.720	6.652	6.669
3 (H)	2.59	2.57	2.58	7.875	7.800	7.823
4 (4-OMe)	2.43	2.40	2.42	9.047	8.960	8.985
5 (4-Oct)	2.42	2.39	2.40	9.594	9.517	9.540

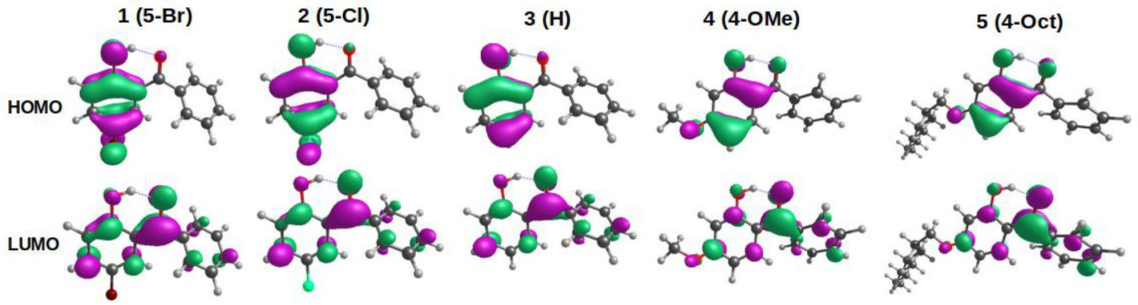

Fig. 4. The HOMO and LUMO of derivative 1 - 5 obtained from B3LYP/6-31 + G(2df,2p) gas phase calculations. A contour of 0.05 eÅ^{-3} was used for the orbital plot. Colour code (online version): C (black), O (red), H (white), Br (burgundy) and Cl (green).

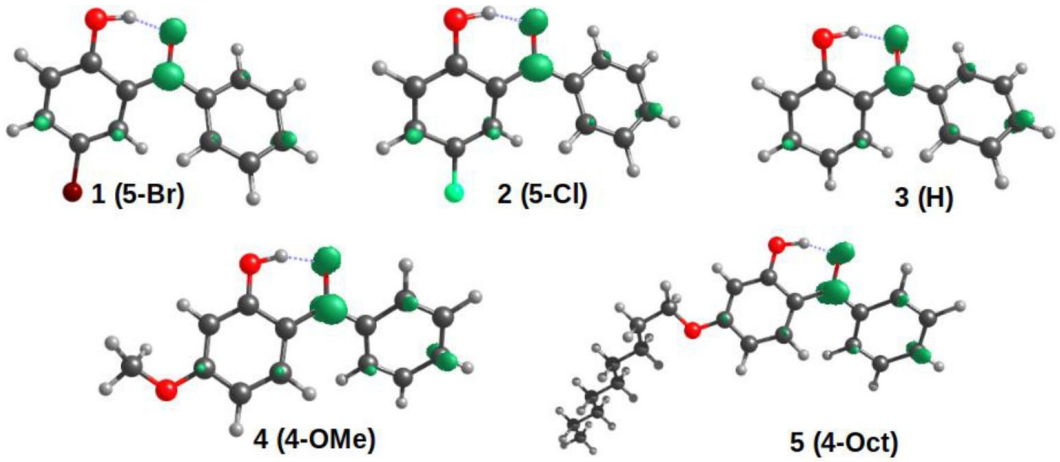

Fig. 5. Spin density profile of the B3LYP/6-31 + G(2df,2p) gas phase optimized reduced molecules 1^- – 5^-, showing the distribution of the added electron of the reduced molecule. A contour of 0.015 eÅ^{-3} was used for the spin plot. Colour code (online version): C (black), O (red), H (white), Br (burgundy) and Cl (green).

molecules 1 and 2 are expected to have the largest reduction (most positive) potential and 5 the lowest reduction (most negative) potential. This is in agreement with experimental observation (see the discussion in the next section).

The calculated dipole moments of 1–5 follow the inverse trend as the calculated electron affinity of 1–5, namely 2 (smallest value) < 1 < 3 < 4 < 5, regardless of the solvent. Fermi and Teller first predicted a minimum dipole moment of 1.625 Debye for an electron to bind to a stationary dipole [29]. Theoretical and experimental studies found that for real molecular systems this critical dipole must be increased implying all molecules in this study can be reduced (uptake of an electron), see dipole moment values in Table 1.

The HOMO and LUMOs of 1–5 are shown in Figure 4, The HOMO of the neutral molecules are mainly located on the hydroxy-substituted phenyl ring (fragment 3 in Figure 1), while the LUMOs are mainly located on the carbonyl group (fragment 2 in Figure 1). Upon reduction of a molecule, the electron will be added to the LUMO, implying reduction will mainly occur on the carbonyl moiety, but also spread over fragment 3 and 1. The spin density profiles of the reduced molecules 1^-–5^-, shown in Figure 5, show that the added electron upon reduction is mainly located on the carbonyl group (i.e. fragment 2, ca 0.536–0.554 e^-), with 0.221–0.318 e^- on the phenyl ring (fragment 1) and the rest (ca 0.129–0.233 e^-) on fragment 3 as defined in Figure 1 and also shown in Table 2. The different solvents did not have a large influence on the electron distribution of the added unpaired electron on the reduced molecule. In all solvent the unsubstituted 2-hydroxybenzophenone, molecule 3 (H), has ca 0.20 e^- on hydroxy-substituted phenyl ring, fragment 3. In all solvent the two molecules with an electron withdrawing substituent, 1 (5-Br) and 2 (5-Cl), in their reduced state, have more electron density on the hydroxy-substituted phenyl ring fragment 3 (ca 0.23 e^-) than the two molecules with an electron donating substituent, 4 (4-Ome) and 5 (4-Oct) (ca 0.13 e^-), in their reduced state.

3.2 Experimental Reduction Potentials

The electrochemical properties of five HBP molecules 1–5, described in Figure 1, were examined using cyclic

Table 2. The Mulliken spin density (e^-) of the derivatives in their reduce state in solvents ACN, DMF and DMSO. Figure 5 visualizes the spin density of the molecules.

	Molecule	Fragment-1	Fragment-2	Fragment-3
ACN	1^- (5-Br)	0.223	0.544	0.232
DMF	1^- (5-Br)	0.226	0.542	0.233
DMSO	1^- (5-Br)	0.225	0.542	0.232
ACN	2^- (5-Cl)	0.221	0.548	0.231
DMF	2^- (5-Cl)	0.223	0.545	0.232
DMSO	2^- (5-Cl)	0.223	0.546	0.232
ACN	3^- (H)	0.265	0.539	0.196
DMF	3^- (H)	0.268	0.536	0.196
DMSO	3^- (H)	0.268	0.536	0.196
ACN	4^- (4-Ome)	0.313	0.546	0.140
DMF	4^- (4-Ome)	0.318	0.543	0.139
DMSO	4^- (4-Ome)	0.317	0.543	0.139
ACN	5^- (4-Oct)	0.314	0.556	0.130
DMF	5^- (4-Oct)	0.318	0.553	0.129
DMSO	5^- (4-Oct)	0.318	0.553	0.129

voltammetry measurements in three solvent media ACN, DMF and DMSO. Representative cyclic voltammograms obtained for the five derivatives in the solvents at scan rates of 0.100 and 0.500 V/s are shown in Figure 6. The values obtained for the peak anodic potential (E_{pa}), peak cathodic potential (E_{pc}), peak separation (ΔE_p) and the corresponding formal reduction potential ($E^{0'}$ in V) at the scan rate of 0.100 V/s are given in Table 3. All the molecules show a very sharp reduction peak with a small re-oxidation peak, except for 1 and 2 in ACN at low scan rates. The re-oxidation peak increases with scan rate, implying that the reduced radical that formed upon reduction is relative stable at high scan rates. The locus of the added electron upon reduction, which is mainly on the carbonyl group, is described in the previous section, also see Figure 5 and Table 2.

The peak cathodic current follows the Randles-Sevcik equation, but the peak current ratios i_{pa}/i_{pc} are small, ca 0.2 for the 0.50 V/s scans, significantly lower than 1 as expected for a chemically reversible process [30,31], see for Figure 7 for HBP molecule 1. The peak separation $\Delta E_p = 0.063$–0.090 V for the 0.100 V/s scans, slightly larger as $\Delta E_p = 0.059$ V expected for a one electron transfer process [32], due to experimental cell imperfections and ohmic drop effects. ΔE_p for the known 1 e^- transfer processes of the Fc^+/Fc couple, used as internal standard were ca 0.06 V. The reduction process of the HBP derivatives could be described as quasi reversible [33–35].

The experimental reduction potential of the derivatives follows the same order in all three solvents, as $1 > 2 > 3 > 4 > 5$ (Figure 6). However, the shift in reduction potential in going from 1 to 5, $\Delta E^{0'} = E^{0'}(5) - E^{0'}(1)$ decreases in going from ACN (0.25 V) to DMF (0.23 V) to DMSO (0.18 V for 0.100 V/s scans). Consequently in DMF and DMSO solvent medium molecules 1 and 2 with electron withdrawing group results into lower reduction potential compared to ACN, while the molecules with electron donating group (4 and 5) in ACN medium give lower reduction potential than DMSO. The order of solvent effect on the derivatives

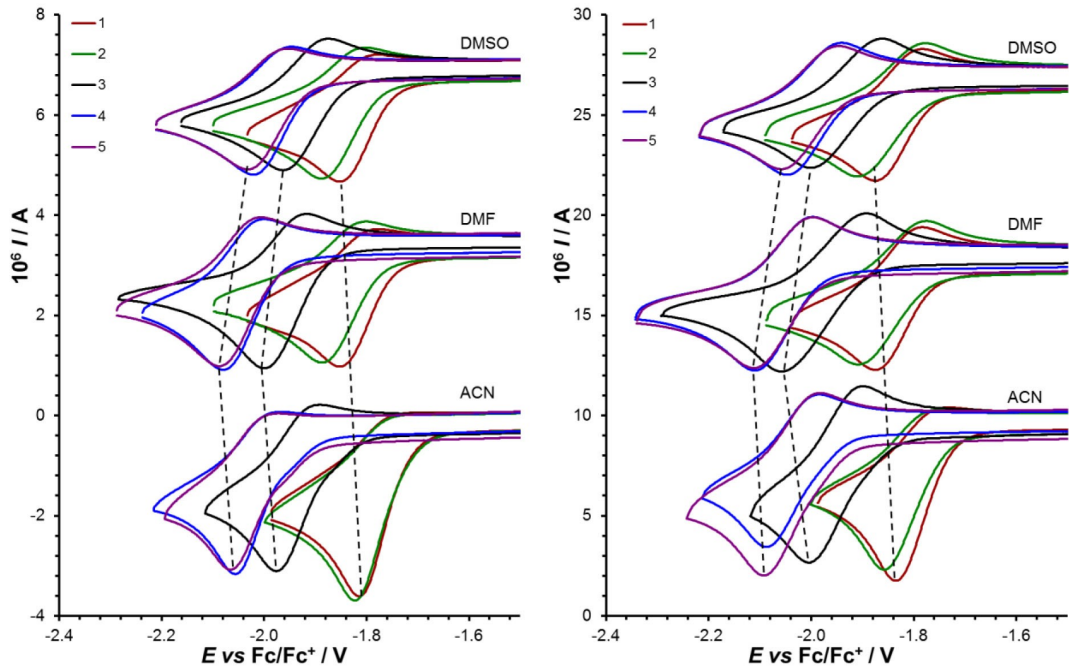

Fig. 6. Cyclic voltammograms of HBP derivatives 1–5, at 0.100 (left) and 0.500 (right) Vs^{-1}. Measurements were done in 0.1 M [NBu_4][PF_6]/solvent, on a glassy carbon working electrode, at 25.0 °C.

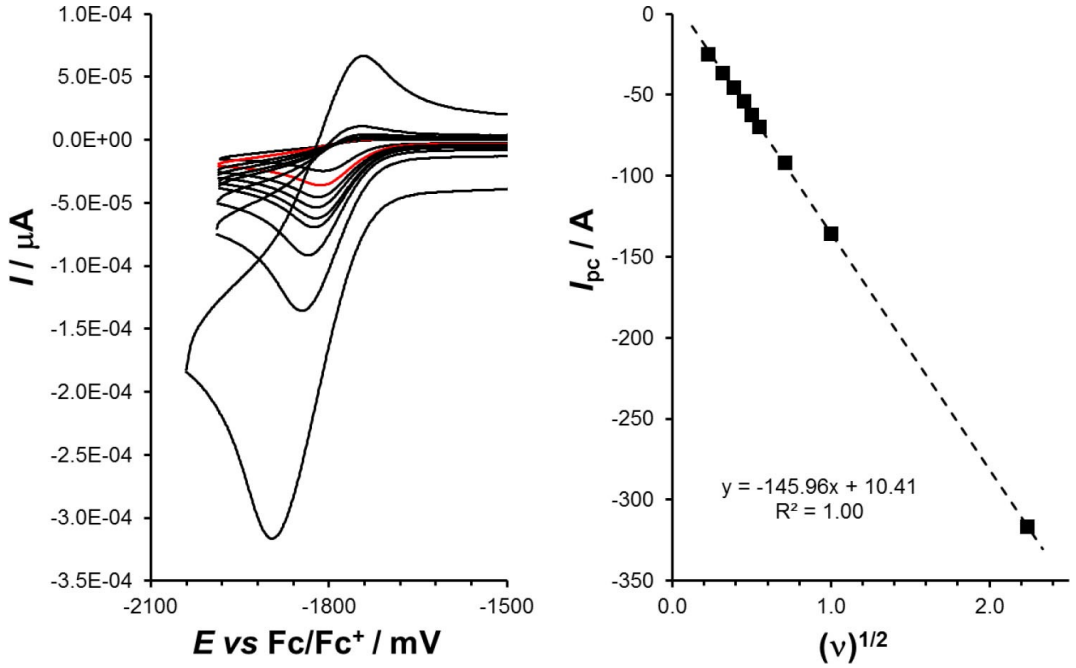

Fig. 7. Left: Cyclic voltammograms of HBP derivative 1 (5-Br), at scan rates of 0.050 (smallest peak current), 0.100 (red), 0.150, 0.200, 0.250, 0.300, 0.500, 1.000, 5.00 (maximum peak current) in Vs^{-1} *vs* Fc/Fc^+. Right: Relationship between the square root of the scan rate $(Vs^{-1})^{1/2}$ and peak cathodic current for complex 1 with $R^2 = 1$, as described by the Randles-Sevcik equation. Measurements were done in 0.1 M $[NBu_4][PF_6]$/ACN, on a glassy carbon working electrode, at 25.0 °C.

with electron withdrawing group is DMF ≈ DMSO < ACN while in derivatives with electron donating group is DMF < ACN < DMSO. In all the molecules, DMF leads to a lower reduction potential compared to ACN (Figure 6 and Table 3). The solvent effect of DMF and DMSO are much significant in molecule 3, 4 and 5 while they are approximately the same in molecules 1 and 2 with electron withdrawing group. The experimental order of the formal reduction potential ($E^{0'}$) of molecule 3 is −1.955 (DMF) < −1.934 (ACN) < −1.917 (DMSO) V *vs* Fc/Fc^+ which is same with that of molecules 4 and 5 (for 5: −2.048 (DMF) < −2.021 (ACN) < −1.990 (DMSO)) but different from that of 1 (−1.813 (DMSO) ≈ −1.819 (DMF) < −1.774 (ACN)) and 2 (−1.844 (DMSO) ≈ −1.840 (DMF) < −1.786 (ACN)).

Hammett substituent constants are used to quantify the electron donating or electron withdrawing property of a substituent on a phenyl ring. A linear relationship between the experimental reduction potential of 1–5 and the Hammett substituent constants [36] for the molecules is obtained, see Figure 8, illustrating good communication between the substituent and the rest of the molecule. There is also a linear trend between the experimental reduction potential (energy needed to promote an electron from the electrode to the analyte) of 1–5 and the calculated electron affinity (the energy change due to the addition of an electron to the molecule) of the molecules, see Figure 8.

Table 3. Experimental peak anodic potential (E_{pa}), peak cathodic potential (E_{pc}), peak separation (ΔE_p) and formal reduction potential ($E^{0'}$ in V) of the complexes from this study in the indicated solvents, at a scan rate of 0.100 V/s reported *vs* Fc/Fc^+.

	E_{pc}(V)	E_{pa}(V)	ΔE_p(V)	$E^{0\prime}$(V)
ACN				
1 (5-Br)	−1.814	−1.735[a]	0.078	−1.774
2 (5-Cl)	−1.821	−1.750[a]	0.071	−1.786
3 (H)	−1.976	−1.892	0.084	−1.934
4 (4-OMe)	−2.056	−1.966	0.089	−2.011
5 (4-Oct)	−2.066	−1.979	0.090	−2.021
DMF				
1 (5-Br)	−1.851	−1.788	0.063	−1.819
2 (5-Cl)	−1.880	−1.800	0.079	−1.840
3 (H)	−1.997	−1.914	0.083	−1.955
4 (4-OMe)	−2.080	−2.000	0.079	−2.040
5 (4-Oct)	−2.087	−2.008	0.079	−2.048
DMSO				
1 (5-Br)	−1.851	−1.776	0.075	−1.813
2 (5-Cl)	−1.886	−1.803	0.083	−1.844
3 (H)	−1.963	−1.872	0.090	−1.917
4 (4-OMe)	−2.019	−1.942	0.077	−1.981
5 (4-Oct)	−2.029	−1.951	0.078	−1.990

[a] Estimated

3.3 Excitation Properties

The experimental UV spectra for 1–5 in the solvents ACN, DMF and DMSO are shown in Figure 9. The

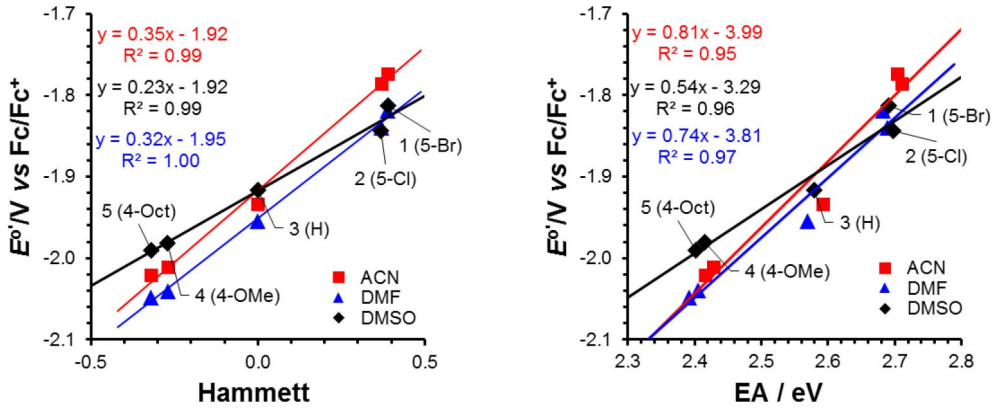

Fig. 8. Relationship between the formal reduction potential, $E^{0'}$ in V *vs* Fc/Fc^+ at 0.100 V s^{-1}, of 1–5 and (left) the Hammett substituent constant of the substituent and (right) the calculated electron affinity of the molecules, in the solvents ACN, DMF and DMSO. Hammett substituent for is 1 ($\sigma_m = 0.39$ for Br), 2 ($\sigma_m = 0.37$ for Cl), 3 ($\sigma = 0$ for H), 4 ($\sigma_p = -0.27$ for OMe), 5 ($\sigma_p = -0.32$ for OBu) [36], calculated electron affinities from Table 1, E_{pc} from Table 3.

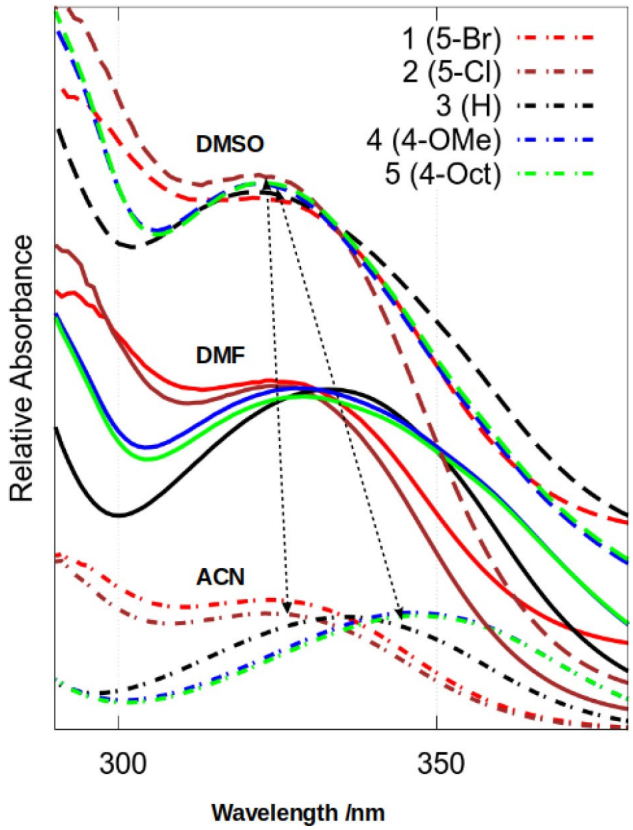

Fig. 9. The experimental UV absorption for all the derivatives in the solvents ACN, DMSO and DMF. The arrows show the trend of the shift of experimental λ_{max} for 1 and 2 (left arrow) and 4 and 5 (right arrow) across the three solvents.

maximum absorption wavelength (λ_{max}) that represent the HOMO to LUMO excitation for all the derivatives are added to Table 4. It is very obvious from the experimental λ_{max} that the solvent effect is more significant in the UV absorption of the derivatives 4 (4-OMe) and 5 (4-Oct) with electron donating group, resulting into a longer wavelength in the solvent ACN in the order of ACN > DMF > DMSO. The same order is also observed in the experimental absorption of the derivative 1 (5-Br) and 2 (5-Cl) and 3 (H) but to a lesser effect compared to that of those with electron donating group. The solvent did not show an effect on the theoretical predicted UV/vis λ_{max}, obtained from TDDFT calculations, see Table 4. Theoretical λ_{max} overestimated the experimental λ_{max} for 1 and 2 by 35–43 nm, while predicting λ_{max} for 3–5 more accurate (within 5–24 nm)

In Table 5 the TDDFT calculated λ_{max} for the HOMO to LUMO excitation of the derivatives with the contribution of the fragment 1, 2 and 3 (Figure 1) to the excitation in ACN are listed. The calculated λ_{max} are largely characterised with HOMO to LUMO excitation as evident from their high percentage contribution (from 94 % to 98 %) as shown in Table 5. The contribution of the fragments to the excitation of the electrons clearly shows that the excitation are mainly from the fragment 3 (54–57 %) to the linking C=O of fragment 2 that connect fragment 3 to 1. The fragment 3 that represent the centre for substitutional change, which differentiates the derivatives from each other is also the fragment that dominate the HOMO of the derivatives (Figure 4). The feature of the HOMO and LUMO shown in Figure 4, also support the electron excitation as the HOMO is predominantly from the distinguishing fragment 3 on the HOMO to both fragments 2 and 1 located on the LUMO.

3.4 HOMO, LUMO and Band Gab

In order to determine the experimental HOMO and LUMO of the derivatives, we make use of the onset values of the experimental CV of the observed reduction potential spectra [24,25] for the LUMO (equation 1) and offset values of the UV [16] spectra for the E_{gap} (equation 2), as shown in Figure 2 for derivative 1

Table 4. The longest wavelength (nm) of the 1–5 in different solvents for the experimental UV/vis and theoretical UV/vis (TD-B3LYP/6-31 + G(2df,2p) calculation in the indicated solvent).

	Exp			TDDFT		
	ACN	DMF	DMSO	ACN	DMF	DMSO
1 (5-Br)	324	324	321	364.1	363.6	363.7
2 (5-Cl)	323	324	322	359.6	359.2	359.2
3 (H)	336	333	321	345.2	344.9	345.0
4 (4-OMe)	346	329	322	334.3	333.7	333.8
5 (4-Oct)	347	329	323	334.9	334.3	334.4

(5-Br). Since no experimental oxidation for the HBP derivatives is measured, no oxidation peak is available for the determination of the HOMO from experimental CV values, thus the UV-Vis spectral data offset was used through the optical E_{gap} expression to determine the experimental HOMO (from equation 2) as explained in the methodology. The values of the experimental HOMO (calculated from equation 2) and LUMO (calculated from equation 1) and selected frontier orbitals of the theoretical model (obtained from the output files of the DFT computations) are added to the supplementary Table S2. The features of the change in the HOMO and LUMO across all the three solvents are shown in Figure 10 for both experimental and theoretical models.

Both experimental and theoretical gave the same order of change in the LUMO energy levels across the derivatives as 5 > 4 > 3 > 2 > 1 indicating that the LUMO of the derivatives with electron withdrawing group falls down to a lower energy level compared to others. In the experimental results, the HOMO also fall to lower energy level for the molecules 1-Br and 2-Cl with electron withdrawing group following the order 5 > 4 > 3 > 2 > 1 (except for 1 and 2 in DMF where the experimental HOMO levels are very similar), but this order is not exactly reproduced by the theoretical calculations that followed the order 5 > 4 > 1 > 2 > 3 in all solvents (Figure 10). The calculated HOMO levels reproduced the experimental HOMO values within 0.2 eV, while the calculated LUMOs overestimated the experimental LUMOs with ca 0.8 eV (data in Table S2).

Table 5. The λ_{max} for the HOMO to LUMO excitation of the derivatives and the contribution of the fragment 1, 2 and 3 to the excitation (B3LYP/6-31 + G(2df,2p) calculation in ACN)

	λ_{max}	f	Excitation type	Excitation type	Frag-1	Frag-2	Frag-3
1 (5-Br)	364.1	0.195	HOMO- > LUMO (98 %)		2– > 19 (17)	2– > 42 (40)	95– > 40 (-55)
2 (5-Cl)	359.6	0.218	HOMO- > LUMO (98 %)		3– > 19 (16)	2– > 41 (39)	95– > 40 (-55)
3 (H)	345.2	0.239	HOMO- > LUMO (97 %)		3– > 20 (17)	3– > 42 (39)	94– > 37 (-57)
4 (4-OMe)	334.3	0.481	HOMO- > LUMO (94 %)	H-1- > LUMO (2 %)	5– > 24 (19)	7– > 43 (36)	88– > 34 (-54)
5 (4-Oct)	334.9	0.504	HOMO- > LUMO (94 %)	H-1- > LUMO (3 %)	5– > 24 (19)	8– > 42 (34)	88– > 34 (-54)

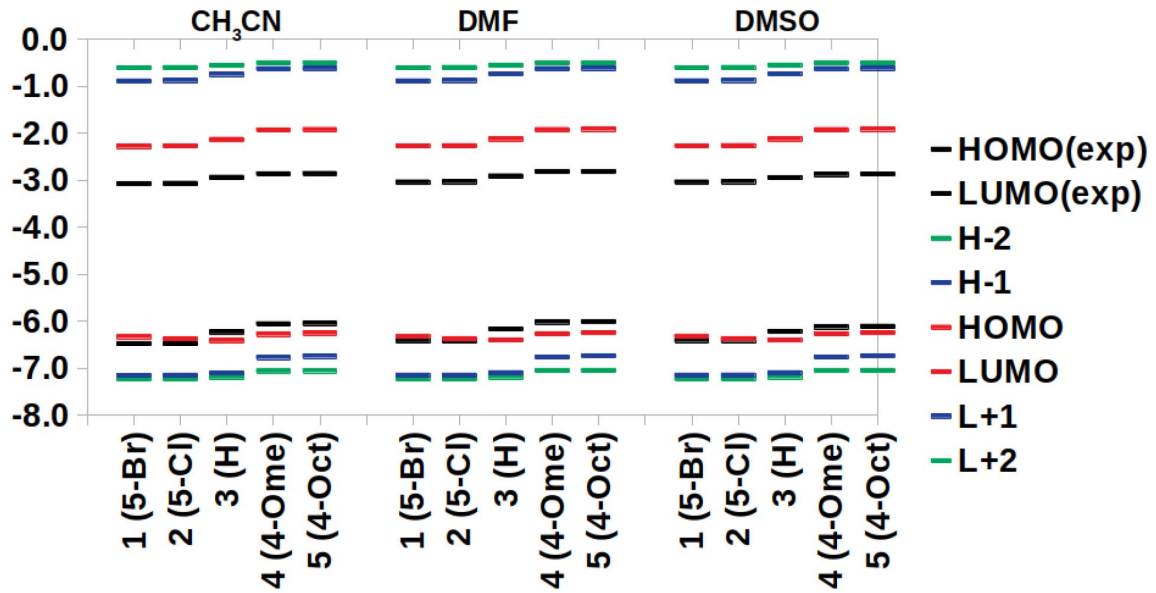

Fig. 10. The energies of the experimental HOMO (calculated from equation 2) and LUMO (calculated from equation 1) plots and the DFT calculated frontier orbitals (obtained from the output files of the DFT computations) in ACN (left), DMF (middle) and DMSO (right) solvents. Y-axis gives energy in eV.

4 Conclusion

This research presents effects of three solvents ACN, DMF and DMSO and the electron donating or withdrawing ability of substituents on 2-hydroxybenzophenone derivatives on the experimental reduction potential, UV absorption, HOMO and LUMO energy level and band gap of five derivatives of HBP. The results of the study showed that:

- The reduction process of the HBP derivatives could be described as quasi reversible since the ratio of the experimental i_{pa}/i_{pc} ration is lower than 1 and the peak separation $\Delta E_p = 0.063–0.090$ V (0.100 V/s scans) is larger than 0.057 V.
- The experimental reduction potential values clearly show that the derivatives with electron withdrawing group (EWG), 1 (5-Br) and 2 (5-Cl), have more favourable reduction potential (higher reduction potential) compared to other derivatives 3 (H), 4 (4-OMe) and 5 (4-Oct).
- The molecules 1 (5-Br) and 2 (5-Cl) with a higher reduction potential, are also are characterised with stronger electron affinity, but lower dipole moment, and HOMO and LUMO energy level values and lower UV absorption wavelength (in ACN and DMF) than the molecules with electron donating groups like 4 (4-OMe) and 5 (4-Oct).
- The type of solvents affect the reduction potential lead order of ACN > DMSO > DMF. The difference between the solvent effects of DMF and DMSO on reduction potential depends on the type of the derivatives. The solvent effect of DMF and DMSO is significant different in molecule 3 (H), 4 (4-OMe) and 5 (4-Oct), while they are approximately the same in molecules (5-Br) and 2 (5-Cl). Solvent effect also affect the experimental UV absorption especially in derivatives with electron donating groups as ACN resulting into longer wavelength values in the order of ACN > DMF > DMSO.

Acknowledgement

The authors are grateful to acknowledge the University of the Free State and the National Research Foundation (NRF) in South Africa for financial support (Grant Nos: 109673, 113327 and 96111). The High-Performance Computing facility of the UFS, the CHPC of South Africa and the Norwegian Supercomputing Program (UNINETT Sigma2, Grant No. NN9684K) are acknowledged for computer time. Open access funding enabled and organized by Projekt DEAL.

References

[1] L. A. Baker, M. D. Horbury, S. E. Greenough, M. N. R. Ashfold, V. G. Stavros, *Photochem. Photobiol. Sci.* **2015**, *14*, 1814–1820.
[2] R. Kumasaka, A. Kikuchi, M. Yagi, *Photochem. Photobiol.* **2014**, *90*, 727–733.
[3] V. G. Stavros, *Nat. Chem.* **2014**, *6*, 955–956.
[4] S. Forestier, *J. Am. Acad. Dermatol.* **2008**, *58*, S133–S138.
[5] A. Ricci, M. N. Chrétien, L. Maretti, J. C. Scaiano, *Photobiol. Sci.* **2003**, *2*, 487–492.
[6] M. T. Ignasiak, C. Houøe-levin, G. Kciuk, B. Marciniak, *ChemPhysChem.* **2015**, *16*, 628–633. doi:10.1002/cphc.201402703.
[7] J. Catalán, J. Palomar, J. L. G. De Paz, *J. Phys. Chem. A* **1997**, *5639*, 7914–7921.
[8] P. J. Cox, S. M. MacManus, *Acta Crystallogr. Sect. C* **2003**, *59*, o603–o604.
[9] K. Saraswat, R. N. Prasad, R. Ratnani, J. E. Drake, M. B. Hursthouse, M. E. Light, *Inorg. Chim. Acta* **2006**, *359*, 1291–1295.
[10] A. Filarowski, A. Kochel, K. Cieslik, A. Koll, *J. Phys. Org. Chem.* **2005**, *18*, 986–993.
[11] S. M. Scalzullo, S. Khorasani, J. P. Michael, *Acta Crystallogr. Sect. E* **2013**, *69*, o139–o139.
[12] C. Cen, G. Chen, C. Han, X. Song, *Acta Crystallogr. Sect. E* **2009**, *69*, o2815–o2815.
[13] A. Mendieta, F. Jiménez, L. Garduño-Siciliano, A. Mojica-Villegas, B. Rosales-Acosta, L. Villa-Tanaca, G. Chamorro-Cevallos, J. L. Medina-Franco, N. Meurice, R. U. Gutiérrez, L. E. Montiel, M. del C. Cruz, J. Tamariz, *Bioorg. Med. Chem.* **2014**, *22*, 5871–5882.
[14] N. Radychev, B. Kempken, C. Krause, J. Li, J. Kolny-Olesiak, H. Borchert, J. Parisi, *Org. Electron.* **2015**, *21*, 92–99.
[15] V. Jessé, R. De Oliveira, E. Assunção, M. Luisa, H. Awada, H. De Santana, R. C. Hiorns, C. Lartigau-dagron, C. De Almeida, *J. Mol. Liq.* **2018**, *268*, 114–121.
[16] C. S. Costa, R. J. S. Taveira, C. F. R. A. C. Lima, *Opt. Mater.* **2016**, *58*, 51–60.
[17] A. B. Murphy, *Sol. Energy Mater. Sol. Cells.* **2007**, *91*, 1326–1337.
[18] B. Ketterer, M. Heiss, M. J. Livrozet, A. Rudolph, E. Reiger, A. Fontcuberta i Morral, *Phys. Rev. B.* **2011**, *83*, 125307.
[19] W. Jin, P.-C. Yeh, N. Zaki, D. Zhang, J. T. Sadowski, A. Al-Mahboob, A. M. van der Zande, D. A. Chenet, J. I. Dadap, I. P. Herman, P. Sutter, J. Hone, R. M. Osgood, *Phys. Rev. Lett.* **2013**, *111*, 106801.
[20] M. Grätzel, *Inorg. Chem.* **2005**, *44*, 6841–6851.
[21] A. M. Smith, S. Nie, *Acc. Chem. Res.* **2010**, *43*,190–200.
[22] A. Guerrero-Corella, F. Esteban, M. Iniesta, A. Martín-Somer, M. Parra, S. Díaz-Tendero, A. Fraile, J. Alemán, *Angew. Chem. Int. Ed.* **2018**, *57*, 5350–5354; *Angew. Chem.* **2018**, *130*, 5448–5452.
[23] G. Gritzner, J. Kuta, *Pure Appl. Chem.* **1984**, *56*, 461–466.
[24] M. Lu, W. Wang, L. Liang, S. Yan, Q. Ling, *Polym. Bull.* **2017**, *74*, 603–614.
[25] C. Lu, Q. Liu, P. Gu, D. Chen, F. Zhou, H. Li, Q. Xu, J. Lu, *Polym. Chem.* **2014**, *5*, 2602.
[26] M. J. Frisch, G. W. Trucks, H. B. Schlegel, G. E. Scuseria, M. A. Robb, J. R. Cheeseman, G. Scalmani, V. Barone, G. A. Petersson, H. Nakatsuji, X. Li, M. Caricato, A. V. Marenich, J. Bloino, B. G. Janesko, R. Gomperts, B. Mennucci, H. P. Hratchian, J. V. Ortiz, A. F. Izmaylov, J. L. Sonnenberg, D. Williams-Young, F. Ding, F. Lipparini, F. Egidi, J. Goings, B. Peng, A. Petrone, T. Henderson, D. Ranasinghe, V. G. Zakrzewski, J. Gao, N. Rega, G. Zheng, W. Liang, M. Hada, M. Ehara, K. Toyota, R. Fukuda, J. Hasegawa, M. Ishida, T. Nakajima, Y. Honda, O. Kitao, H. Nakai, T. Vreven, K. Throssell, J. Montgomery, J. A., J. E. Peralta, F. Ogliaro, M. J. Bearpark, J. J. Heyd, E. N.

Brothers, K. N. Kudin, V. N. Staroverov, T. A. Keith, R. Kobayashi, J. Normand, K. Raghavachari, A. P. Rendell, J. C. Burant, S. S. Iyengar, J. Tomasi, M. Cossi, J. M. Millam, M. Klene, C. Adamo, R. Cammi, J. W. Ochterski, R. L. Martin, K. Morokuma, O. Farkas, J. B. Foresman, D. J. Fox, *Gaussian 16, Revision B.01*, **2016**.
[27] A. V. Marenich, C. J. Cramer, D. G. Truhlar, *J. Phys. Chem. B.* **2009**, *113*, 6378–6396.
[28] R. E. Skyner, J. L. Mcdonagh, C. R. Groom, T. Van Mourik, *Phys. Chem. Chem. Phys.* **2015**, *17*, 6174–6191.
[29] E. Fermi, E. Teller, *Phys. Rev.* **1947**, *72*, 399–408.
[30] N. Elgrishi, K. J. Rountree, B. D. McCarthy, E. S. Rountree, T. T. Eisenhart, J. L. Dempsey, *J. Chem. Educ.* **2018**, *95*, 197–206.
[31] P. T. Kissinger, W. R. Heineman, *J. Chem. Educ.* **1983**, *60*, 702–706.
[32] H. J. Gericke, N. I. Barnard, E. Erasmus, J. C. Swarts, M. J. Cook, M. A. S. Aquino, *Inorg. Chim. Acta* **2010**, *363*, 2222–2232.
[33] R. L. Birke, M.-H. Kim, M. Strassfeld, *Anal. Chem.* **1981**, *53*, 852–856.
[34] M. V. Mirkin, A. J. Bard, *Anal. Chem.* **1992**, *64*, 2293–2302.
[35] J. C. Myland, K. B. Oldham, *Electrochem. Commun.* **2005**, *7*, 282–287.
[36] C. Hansch, A. Leo, R. W. Taft, *Chem. Rev.* **1991**, *91*, 165–195.

Received: May 4, 2020
Accepted: June 18, 2020
Published online on July 14, 2020

